Circuits, Systems, and Signal Processing (2021) 40:5654–5681
https://doi.org/10.1007/s00034-021-01740-7

Adaptive S-Transform with Chirp-Modulated Window and Its Synchroextracting Transform

Bei Li[1] · **Zhuosheng Zhang**[1] · **Xiangxiang Zhu**[1]

Received: 24 December 2020 / Revised: 22 April 2021 / Accepted: 26 April 2021 / Published online: 31 May 2021

Abstract

In this paper, an adaptive S-transform with chirp-modulated window (ASTCMW) is proposed to improve the energy concentration of the S-transform using the rotation of a function which is the inverse fractional Fourier transform of the chirp-modulated window. The window contains two parameters, the chirp rate parameter and the frequency parameter. The chirp rate parameter varying over time and frequency can control the rotation of the function in the time–frequency plane, and it can be determined by maximizing the amplitude of the ASTCMW. The frequency parameter assists the chirp rate parameter to rotate the function at high frequencies, and it is analyzed by the match between the input signal and the chirp-modulated window. The ASTCMW improves greatly the energy concentration in the instantaneous frequency in noiseless and noisy environments. Furthermore, the instantaneous frequency equation based upon the ASTCMW is developed, and then, a synchroextracting transform is proposed. By extracting the time–frequency points satisfying the equation, the proposed synchroextracting transform sharpens the ASTCMW result and gives a high-resolution time–frequency representation. The experiment results demonstrate the effectiveness of the ASTCMW and the proposed synchroextracting transform.

Keywords Adaptive S-transform · Chirp-modulated window · Fractional Fourier transform · Synchroextracting transform

✉ Zhuosheng Zhang
zszhang@mail.xjtu.edu.cn

Bei Li
libeixjtu@163.com

Xiangxiang Zhu
zhuxiangxiang@stu.xjtu.edu.cn

[1] School of Mathematics and Statistics, Xi'an Jiaotong University, Xi'an 710049, China

1 Introduction

In many applications, such as mechanical engineering [24,38,45], seismic [42], and biomedicine [32], it is important to obtain the features of a non-stationary signal. The time-varying information, especially the instantaneous frequency (IF) which describes the significant physical parameter of the input signal, plays a prominent role in these features. The time–frequency analysis (TFA) method is an efficient tool for the representation of the IF. Accordingly, many various TFA methods have been developed in the last few decades. Some widely used methods of them are classical TFA methods. Ordinarily, they are separated into two categories: the quadratic TFA methods and the linear TFA methods. In classical quadratic TFA methods, such as the Wigner–Ville distribution (WVD), the cross-terms reduce the readability of the time–frequency representation (TFR) of the input signal containing more than one component. In classical linear TFA methods, such as the short-time Fourier transform (STFT) and the continuous wavelet transform (CWT), a high time and frequency resolution cannot be achieved simultaneously in the time–frequency plane because of the Heisenberg uncertainty principle.

The S-transform (ST) [34] can be considered as a hybrid between the STFT and the CWT [39] (i.e., the phase-corrected CWT or the STFT with a window width varying over frequency). It is widely employed in many scientific applications [4,21,30,33,47]. However, the width of the ST window will decrease as the frequency increases. It leads to a poor time resolution at low frequencies and a poor frequency resolution at high frequencies in the time–frequency plane [49]. To overcome the drawback, several modifications were proposed. Some of them are based on the fact that the ST window can be interpreted as the Gaussian window with the standard deviation varying over frequency. To permit users to specify time and frequency resolution [19], the frequency in the standard deviation was modified as the product of the frequency and the inverse of a parameter [27]. In [31], a different parameter controlling the window width was introduced in the original standard deviation. In [41], Wang proposed the adaptive Generalized S-transform combining the above two modifications. To get better progressive control of the window width, the parameter in [27] was modified as the form varying linearly over frequency [2]. In 2015, Moukadem generalized the above modifications [2,19,27,31,41] by introducing a new standard deviation with four parameters [20], and the optimal parameters of this method are acquired by solving an optimization problem. In [49], Zidelmal proposed the S-transform based on compact support kernel (CSK-ST) that contained a compact support kernel instead of the Gaussian window in the ST, and the parameters in the kernel are selected by optimizing the energy concentration. It is worth noting that metaheuristic algorithms [29,36] (nature inspired) are very powerful for an optimization problem. Consequently, a combination of metaheuristic algorithms and parameter selection is promising. Besides, some complex windows were applied to the ST [25,28], and Pinnegar in [26] presented the bi-Gaussian S-transform (bi-Gaussian ST) which contains an asymmetric window composed of two half Gaussians. To preserve the amplitude and frequency, Wang proposed an amplitude- and frequency-preserving S transform [40]. Nevertheless, all of the above methods are based on the width modification of the ST window varying over frequency. In this paper, an adaptive S-transform with chirp-modulated window

(ASTCMW) is proposed, and it is based on a rotation window rather than the width modification of the ST window to match the input signal. The proposed ASTCMW achieves more concentrated energy representation around the IF track than most of the modified methods above.

On the other hand, to enhance the energy concentration in the time–frequency plane, many post-processing methods based upon existing TFA methods have been developed. The reassignment method [12,15,16], first introduced in the 1970s, shifts the location of the energy in each window from the result generated by the STFT or CWT to the barycenter of the window. In 2011, a post-processing method, the synchrosqueezing transform (SST) [10], was presented. It can not only concentrate the energy but also reconstruct the input signal. Subsequently, the synchrosqueezing S-transform (SSST) [14], the Fourier-based synchrosqueezing transform [23], the synchrosqueezing generalized S-transform (SSGST) [42], and the second-order synchrosqueezing transform (Second-SST) [22] were proposed. Inspired by the SST, the synchroextracting transform (SET) [43] was developed. The SET retains the information of the IF and removes most smeared energy in the time–frequency plane. Compared with the SST, the SET gives a more concentrated energy representation for the input signals that have fast varying IF [17]. Following the idea of the SET, in this paper, a new synchroextracting transform based upon the ASTCMW (SET-ASTCMW) is proposed for strongly modulated signals, and it is a post-processing method. The proposed SET-ASTCMW provides a better result than the frequently used post-processing methods.

In practical application, external disturbances, modeling errors, and uncertainties are common, and they can affect the energy concentration and the stability of the solution. To cope with the problem, some methods have been proposed [11,35,37,46]. In particular, for removing noise interference, some methods have been developed [3,13,18]. So robustness of TFA methods is an important property in practice. In this regard, the proposed SET-ASTCMW can give a more robust result.

The rest of the paper is organized as follows. After a brief revisit of the subsistent ST, the ASTCMW is introduced in Sect. 2. Two parameters of the chirp-modulated window, i.e., the chirp rate parameter and the frequency parameter, are discussed in this section. To acquire a clearer TFR for strongly modulated signals, the SET-ASTCMW is developed in Sect. 3. Experimental validations are presented in Sect. 4 followed by drawing the conclusions in Sect. 5.

2 Adaptive S-Transform with Chirp-Modulated Window

In this section, the ASTCMW is introduced first, and then, the estimation of the chirp rate parameter and selection of the frequency parameter are discussed, respectively.

2.1 The Proposed Adaptive S-Transform

The ST of a signal $f(t) \in L^2(R)$ is defined by

$$F(t,\omega) = \int_{-\infty}^{+\infty} f(\tau) g^*(t-\tau,\omega) e^{-j2\pi\omega\tau} \mathrm{d}\tau, \tag{1}$$

where the superscript asterisk * denotes the complex conjugate and $g(t,\omega)$ is the analysis window, which is chosen as Gaussian function

$$g(t,\omega) = \frac{|\omega|}{\sqrt{2\pi}} e^{-\frac{t^2\omega^2}{2}}. \tag{2}$$

Therefore, the ST (1) can be rewritten as [34]

$$F(t,\omega) = \int_{-\infty}^{+\infty} f(\tau) \frac{|\omega|}{\sqrt{2\pi}} e^{-\frac{(t-\tau)^2\omega^2}{2}} e^{-j2\pi\omega\tau} \mathrm{d}\tau. \tag{3}$$

The ST (3) shows that its analysis window varies over frequency. For any input signal, the width of the window is wider at low frequencies and narrower at high frequencies, and it does not take the time–frequency characteristics of the signal into consideration. This leads the ST to suffer from poor time–frequency resolution for many applications. Hence, many modified methods of the ST have been proposed. Most of the studies in the existing literature focus on adapting the width of the window to the signal in order to achieve the TFR of high energy concentration. In this paper, we proposed an adaptive S-transform with chirp-modulated window (ASTCMW), which is defined as follows

$$S(t,\omega,c(t,\omega)) = \int_{-\infty}^{+\infty} f(\tau)(g(t-\tau,\frac{\omega}{\alpha}) e^{j2\pi\frac{c(t,\omega)(t-\tau)^2}{2}})^* e^{-j2\pi\omega\tau} \mathrm{d}\tau, \tag{4}$$

where $g(t,\omega)$ is Gaussian function, as defined in (2), $\alpha > 0$ is a frequency parameter and $c(t,\omega)$ is chirp rate parameter. Particularly, if $c(t,\omega)$ takes a constant and $\alpha = 1$, the ASTCMW is similar to formula (19) in [28]. The proposed transform is adaptive, and its window function can be given as

$$w(t,\omega) = g(t,\frac{\omega}{\alpha}) e^{j2\pi\frac{c(t,\omega)t^2}{2}}. \tag{5}$$

The parameters α and $c(t,\omega)$ of the window are signal dependent. The parameter α controls the width of window $g(t,\frac{\omega}{\alpha})$. The selection of α is analyzed by the fractional Fourier transform (FrFT). The parameter $c(t,\omega)$ is time–frequency-varying and controls the rotation of the function whose FrFT is $w(t,\omega)$. The optimal $c(t,\omega)$ can be achieved by maximizing the amplitude of ASTCMW. It is easy to show that the chirp-modulated window $w(t,\omega)$ satisfied the fourth condition of complex window design in [28], and it makes the TFR of the analyzed signal concentrate on the IF track of the signal in the time–frequency plane.

To further demonstrate the performance of the window $w(t,\omega)$, a linear frequency-modulated (LFM) signal $f(t) = e^{j2\pi t^2}$ is considered. For this signal, the optimal $c(t,\omega)$ can be taken as $c(t,\omega) = 2$, the chirp rate of the signal. In Fig. 1, the WVDs of the signal $f(t)$, the window $g(t,\omega)$, and the window $w(t,\omega)$ with the same $c(t,\omega) = 2$ and different frequency parameters are shown. The WVD of $f(t)$ is a straight line in the time–frequency plane and the WVD of the window $w(t,\omega)$ is a 2D Gaussian function with shape depending on the chirp rate $c(t,\omega)$ and the frequency parameter α. Figure 1b presents the result of the chirp-modulated window $w(t,\omega)$ with $\alpha = 1$ at low frequency. Compared with Fig. 1a, the window yields less blurring effect on the signal $f(t)$ than ST window $g(t,\omega)$. Figure 1d provides the WVD of the window $w(t,\omega)$ with $\alpha = 1$ at high frequency. By comparison with the ST window in Fig. 1c, the chirp-modulated window has a limited effect. In this case, the ASTCMW gives a poor resolution at high frequency. To ameliorate this situation, α is set to 8 in $w(t,\omega)$, and the WVD of $w(t,\omega)$ is displayed in Fig. 1e. Obviously, the chirp-modulated window can match well with the LFM signal overall the time–frequency plane if α is properly adjusted.

For a more general mono-component signal $f(t) = A(t)e^{j2\pi\phi(t)}$, its chirp rate varies over time. Hence, the optimal $c(t,\omega)$ should also vary over time and be taken as the chirp rate.

2.2 Estimation of the Chirp Rate Parameter

A crucial question in the proposed ASTCMW is how to determine the time–frequency-varying parameter $c(t,\omega)$ in order to well match the true chirp rate of the input signal. In this subsection, a discrete algorithm is given, and it gets the estimation of the optimal $c(t,\omega)$, i.e., the chirp rate.

Consider a mono-component signal $f(t)$ modeled as

$$f(t) = A(t)e^{j2\pi\phi(t)}, \tag{6}$$

where $A(t) > 0$ and $\phi(t)$ are the instantaneous amplitude and instantaneous phase, respectively. $\phi'(t)$ is the IF of $f(t)$ and $\phi''(t)$ is the chirp rate of $f(t)$.

By inserting (6) into (4), it is easy to show that

$$\begin{aligned} &S(t,\omega,c(t,\omega)) \\ &= \int_{-\infty}^{+\infty} f(\tau)\frac{|\omega|}{\sqrt{2\pi}\alpha}e^{-\frac{\omega^2(t-\tau)^2}{2\alpha^2}}e^{-j2\pi\frac{c(t,\omega)(t-\tau)^2}{2}}e^{-j2\pi\omega\tau}\mathrm{d}\tau \\ &= \int_{-\infty}^{+\infty} f(t+\tau)\frac{|\omega|}{\sqrt{2\pi}\alpha}e^{-\frac{\omega^2\tau^2}{2\alpha^2}}e^{-j2\pi\frac{c(t,\omega)\tau^2}{2}}e^{-j2\pi\omega(t+\tau)}\mathrm{d}\tau \\ &= \int_{-\infty}^{+\infty} A(t+\tau)e^{j2\pi\phi(t+\tau)}\frac{|\omega|}{\sqrt{2\pi}\alpha}e^{-\frac{\omega^2\tau^2}{2\alpha^2}}e^{-j2\pi\frac{c(t,\omega)\tau^2}{2}}e^{-j2\pi\omega(t+\tau)}\mathrm{d}\tau. \end{aligned} \tag{7}$$

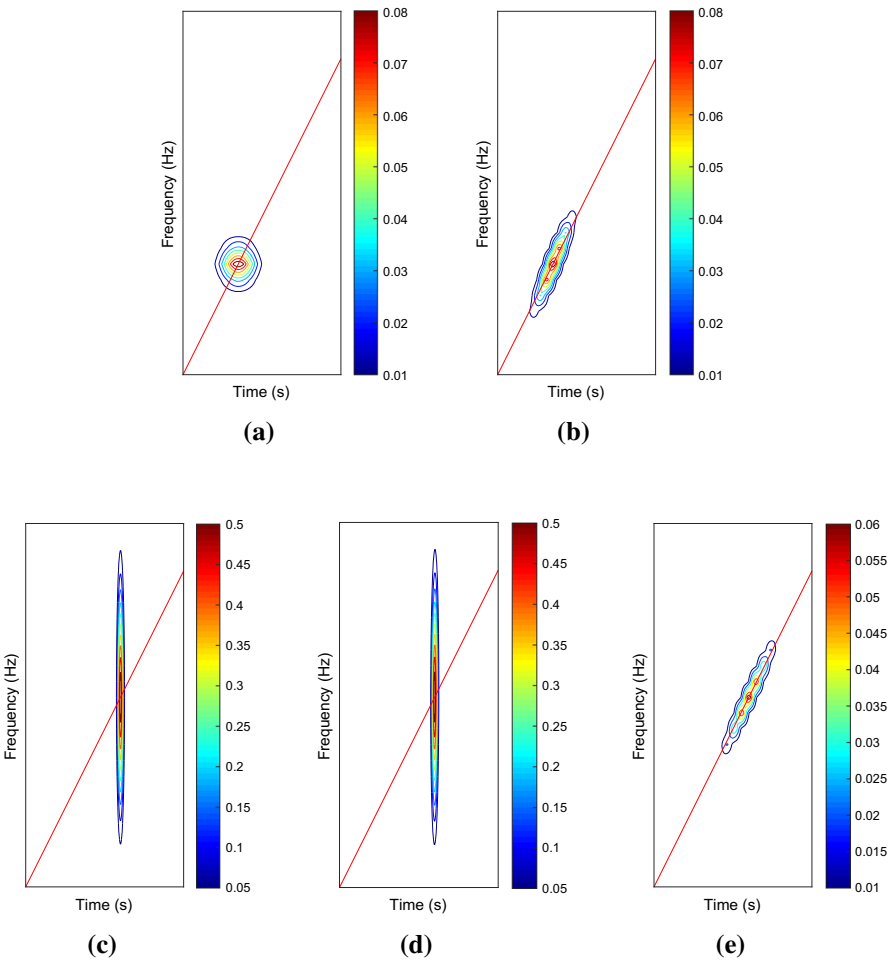

Fig. 1 WVDs of the LFM signal and the window functions. **a** The ST window at $(t, \omega) = (0.5, 1)$, **b** the chirp-modulated window with $c(t, \omega) = 2$ and $\alpha = 1$ at $(t, \omega) = (0.5, 1)$, **c** the ST window at $(t, \omega) = (3, 6)$, **d** the chirp-modulated window with $c(t, \omega) = 2$ and $\alpha = 1$ at $(t, \omega) = (3, 6)$, **e** the chirp-modulated window with $c(t, \omega) = 2$ and $\alpha = 8$ at $(t, \omega) = (3, 6)$

For a small constant $\varepsilon > 0$ and all $t \in (-\infty, \infty)$, if $|\phi'''(t)| < \varepsilon$, then the signal $f(t+\tau) = A(t+\tau)e^{j2\pi\phi(t+\tau)}$ around the point t can be expressed approximately as

$$A(t+\tau)e^{j2\pi\phi(t+\tau)} \approx A(t+\tau)e^{j2\pi(\phi(t)+\phi'(t)\tau+\frac{\phi''(t)}{2}\tau^2)}. \tag{8}$$

By substituting (8) in (7), the amplitude of the ASTCMW in the IF $\omega = \phi'(t)$ satisfies that

$$\begin{aligned} &|S(t,\phi'(t),c(t,\omega))| \\ &\approx |\frac{\phi'(t)}{\sqrt{2\pi}\alpha}\int_{-\infty}^{+\infty} A(t+\tau)e^{-\frac{(\phi'(t))^2\tau^2}{2\alpha^2}}e^{-j2\pi\frac{(c(t,\omega)-\phi''(t))}{2}\tau^2}\mathrm{d}\tau| \\ &\leq |\frac{\phi'(t)}{\sqrt{2\pi}\alpha}\int_{-\infty}^{+\infty} A(t+\tau)e^{-\frac{(\phi'(t))^2\tau^2}{2\alpha^2}}\mathrm{d}\tau|. \end{aligned} \tag{9}$$

The inequality (9) shows that the ASTCMW amplitude in the IF will take the maximum under a certain condition when $c(t,\omega)$, which can be seen as a constant for each (t,ω), is consistent with the chirp rate of the input. According to this fact, $c(t,\omega)$ can be approximated using a method similar to the one in [44]. For each time–frequency point (t,ω), the best argument $c(t,\omega)$ is obtained by

$$\widetilde{c}(t,\omega) \approx \arg\max_{\eta} |S(t,\omega,\eta)|, \tag{10}$$

where η denotes a constant. Like the approach in [44,48], η is considered as

$$\eta = \frac{W_f}{2T_f}\tan(\theta), \quad \theta \in \left(-\frac{\pi}{2},\frac{\pi}{2}\right), \tag{11}$$

where W_f is the sampling frequency of the input signal and T_f is the sampling time of the input.

In the discrete case, suppose that θ has N_θ values, and then, θ_n can be given by

$$\theta_n = -\frac{\pi}{2} + \frac{n\pi}{N_\theta+1}, \quad n = 1,2,\ldots,N_\theta. \tag{12}$$

For each time–frequency point (t,ω), the ASTCMW with respect to parameter θ_n can be rewritten as

$$S(t,\omega,\theta_n) = \int_{-\infty}^{+\infty} \frac{|\omega|}{\sqrt{2\pi}\alpha} f(\tau+t)e^{-\tau^2(\frac{\omega^2}{2\alpha^2}+j\pi\frac{W_f}{2T_f}\tan(\theta_n))}e^{-j2\pi\omega(\tau+t)}\mathrm{d}\tau. \tag{13}$$

By inserting (13) into (10), the discrete approximate value of $c(t,\omega)$ can be achieved.

In theory, the chirp rate $\phi''(t)$ of a mono-component signal can take only one value when t is fixed, and $\widetilde{c}(t,\omega)$ may take more values for the fixed t because of the variation of ω. In the experiment, the multiple values of $\widetilde{c}(t,\omega)$ have a little change, which can be ignored, around the IF for the fixed t. Consequently, $\widetilde{c}(t,\omega)$ can be seen as an approximation of the chirp rate of a mono-component signal.

It is noteworthy that the above technique also can be utilized to deal with a multi-component signal $f(t) = \sum_{n=1}^{N} A_n(t)e^{j2\pi\phi_n(t)}$ if the IFs of the components are separable [22].

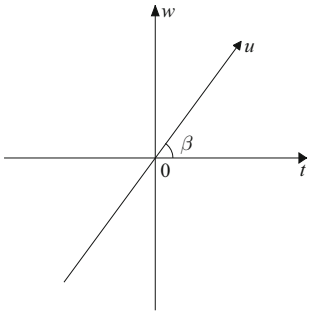

Fig. 2 FrFT rotation in the time–frequency plane

2.3 Analysis for the Frequency Parameter

In this subsection, the selection of parameter α in the chirp-modulated window will be discussed using the FrFT, which is a generalization of the Fourier transform.

Firstly, the FrFT of a signal or function $x(t) \in L^2(R)$ is defined as [1,5]

$$X_\beta(u) = \int_{-\infty}^{+\infty} x(t) K_\beta(t,u) \mathrm{d}t \tag{14}$$

with the transform kernel

$$K_\beta(t,u) = \begin{cases} \sqrt{1-j\cot\beta}\; e^{j2\pi \frac{(t^2+u^2)}{2}\cot\beta - j2\pi tu\csc\beta} & \beta \neq m\pi, \\ \delta(t-u) & \beta = 2m\pi, \\ \delta(t+u) & \beta = (2m-1)\pi, \end{cases} \tag{15}$$

where $m \in Z$. The FrFT corresponds to the counterclockwise rotation by an angle β in the time–frequency plane, as displayed in Fig. 2. When $\beta = \frac{\pi}{2}$, the FrFT is the Fourier transform, and when β takes a negative value, the FrFT corresponds to a clockwise rotation. Without loss of generality, $-\frac{\pi}{2} \leq \beta \leq \frac{\pi}{2}$ is considered here. It is not hard to see that the transform kernel has the following properties [1]:

$$\begin{aligned} K_{-\beta}(t,u) &= K_\beta^*(t,u), \\ K_\beta(t,u) &= K_\beta(u,t). \end{aligned} \tag{16}$$

The inverse FrFT of $X_\beta(u)$ can be written as

$$x(t) = \int_{-\infty}^{+\infty} X_\beta(u) K_{-\beta}(u,t) \mathrm{d}u = \int_{-\infty}^{+\infty} X_\beta(u) K_\beta^*(t,u) \mathrm{d}u. \tag{17}$$

For an LFM signal with a constant chirp rate $c \neq 0$, the chirp-modulated window of its ASTCMW satisfies $c(t,\omega) = c$. According to (17), the inverse FrFT of the above

chirp-modulated window is calculated as follows:

$$\begin{aligned} h(u) &= \int_{-\infty}^{+\infty} g(t, \frac{\omega}{\alpha}) e^{j2\pi \frac{ct^2}{2}} K_\beta^*(t,u)\mathrm{d}t \\ &= \int_{-\infty}^{+\infty} \frac{|\omega|}{\alpha\sqrt{2\pi}} e^{-\frac{t^2\omega^2}{2\alpha^2}} e^{j2\pi \frac{ct^2}{2}} K_\beta^*(t,u)\mathrm{d}t \\ &= \sqrt{\frac{|\omega|^2(1+j\cot\beta)}{\omega^2 - j2\pi\alpha^2(c-\cot\beta)}} e^{-j\pi u^2 \cot\beta} e^{-\frac{2\pi^2\alpha^2\csc^2\beta}{\omega^2 - j2\pi\alpha^2(c-\cot\beta)}u^2}, \end{aligned} \tag{18}$$

where ω is considered as a constant. If the angle satisfies $\beta = \arctan\frac{1}{c}$, $h(u)$ can be rewritten to

$$\begin{aligned} h(u) &= \sqrt{\frac{|\omega|^2(1+j\cot\beta)}{\omega^2}} e^{-j\pi u^2\cot\beta} e^{-2\pi^2\frac{\alpha^2\csc^2\beta}{\omega^2}u^2} \\ &= \sqrt{\frac{|\omega|^2(1+jc)}{\omega^2}} e^{-j\pi u^2 c} e^{-2\pi^2\frac{\alpha^2(c^2+1)}{\omega^2}u^2}. \end{aligned} \tag{19}$$

Equation (19) implies that the chirp-modulated window can be regarded as the FrFT of the function $h(u)$ when a signal with a constant chirp rate is dealt with. In other words, the chirp-modulated window should be considered as the rotation of $h(u)$, and the rotated angle is β. However, $\beta = \arctan\frac{1}{c}$ is fixed because, for an input signal, the chirp rate is certain. Accordingly, for a fixed ω, $h(u)$ only depends on α to make the shape of its rotation, the chirp-modulated window, match with the signal. In order to illustrate the match relationship, the LFM signal $f(t) = e^{j2\pi t^2}$, which has a constant chirp rate, is considered, and its WVD is a straight line in the time–frequency plane, as shown in Fig. 3. In addition, the WVDs of $h(u)$ with different α are displayed in Fig. 3a–c. It is not hard to see that these WVDs are prolonged in different lines. This leads to that the match relationship between the rotation of the WVD of $h(u)$, which is the WVD of the chirp-modulated window, and the WVD of the signal is different, as shown in Fig. 3d–f. More specifically, the chirp-modulated window with $\alpha = 8$ (Fig. 3f) yields less blurring effect than $\alpha = 2$ (Fig. 3d) and $\alpha = 6$ (Fig. 3e). Furthermore, the blurring effect will be less when α takes a higher value. It means that α should take a high value for any signal to obtain a concentrated energy representation in the time–frequency plane. However, if α takes a too high value, the TFR will overflow. Consequently, in this paper, $1 \le \alpha \le 8$ is used.

The above conclusion, however, is based on fixed ω. Under the condition that ω changes, $\frac{\alpha^2(c^2+1)}{\omega^2}$ in (19) should have a higher value than c according to the property of the function $h(u)$ [6]. It means

$$\frac{\alpha^2(c^2+1)}{\omega^2 c} = \gamma > 1. \tag{20}$$

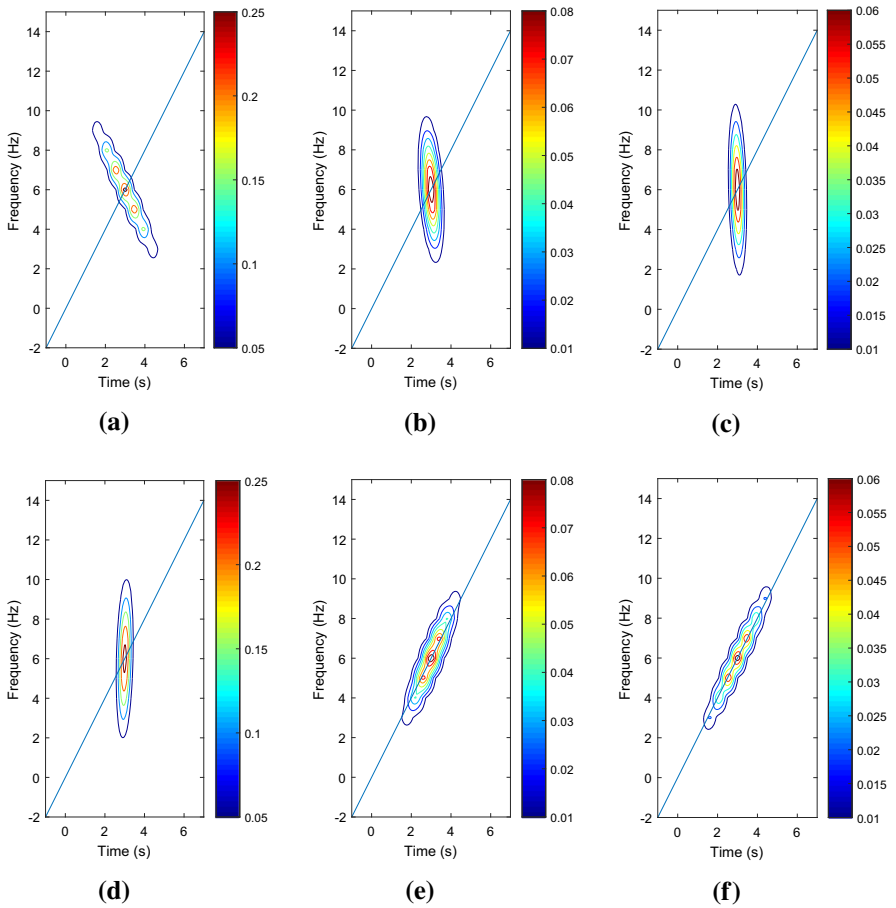

Fig. 3 WVDs of $h(u)$ with $c = 2$ and $\omega = 6$ and the chirp-modulated window at $(t, \omega) = (3, 6)$. **a** $h(u)$ with $\alpha = 2$, **b** $h(u)$ with $\alpha = 6$, **c** $h(u)$ with $\alpha = 8$, **d** the chirp-modulated window with $\alpha = 2$, **e** the chirp-modulated window with $\alpha = 6$, **f** the chirp-modulated window with $\alpha = 8$

There is the same problem as above. If γ takes a higher value, the chirp-modulated window will match well with the signal, whereas if α takes a too high value to make $\gamma >> 1$, the TFR will overflow. Consequently, α should take a proper value for given c and ω, and $1 \leq \alpha \leq 8$ is suggested. However, for a given signal, the optimal selection of the frequency parameter for the ASTCMW depends on the signal. In this regard, one can select the frequency parameter from $1 \leq \alpha \leq 8$ or prior estimation.

It should be noticed that the above discussion is based on a signal with a constant chirp rate, an LFM signal. For a signal with a variable chirp rate, α also can be determined by the above discussion. That is because a signal with a variable chirp rate can be approximated by a series of LFM signals. In fact, the IF is the main feature for the input signal in the time–frequency plane. The IF of the input signal with a variable chirp rate can be locally approximated by its tangent line, and the tangent lines can be viewed as the IF of the LFM signal which has the chirp rate the same as the input

at the tangent point. In other words, the input signal can locally be regarded as an approximately LFM signal, as shown in formula (8).

2.4 Pseudocode for the ASTCMW

To state clearly the ASTCMW, the detailed procedure of the ASTCMW is summarized in Algorithm 1.

Algorithm 1 ASTCMW algorithm

1: Input signal $f(t)$, N_θ (i.e., the number of discrete θ) and the frequency parameter α;
2: Calculate $\theta_n, n = 1, 2, \ldots, N_\theta$, from (12);
3: For each θ_n
4: Calculate the ASTCMW $S(t, \omega, \theta_n)$ from (13);
5: **for** each time–frequency point (t, ω)
6: Define $\widetilde{c}(t, \omega) = \arg\max_{\theta_n} |S(t, \omega, \theta_n)|$;
7: Calculate $S(t, \omega, \widetilde{c}(t, \omega))$;
8: **end for**
9: Output $S(t, \omega, \widetilde{c}(t, \omega))$.

The computational cost of the ASTCMW is obtained by the following procedure under the assumption of a signal with N samples. The ASTCMW with fixed θ_n has to be computed N_θ times, as shown at steps 3, 4 of Algorithm 1, and the computation is $O(N_\theta N^2 \log_2 N)$. Then, an $N_\theta \times N/2 \times N$ matrix is obtained. From this matrix, the maximum detection (i.e., steps 6, 7 in Algorithm 1) requires $O(N_\theta N^2)$ operations. Therefore, the computational complexity of the ASTCMW should be $O(N_\theta N^2 \log_2 N)$.

3 Synchroextracting Transform Based Upon the ASTCMW

The SET is a recently developed high-resolution TFA method, which extracts the IF information and removes smeared energy in the time–frequency plane. In this section, on the basis of the SET and the proposed ASTCMW, a new TFA method is proposed and called SET-ASTCMW.

The IF equation based on the ASTCMW, the key step of the SET-ASTCMW, is stated in the following Theorem.

Theorem 1 *Consider a mono-component signal* (6)*. For a small constant* $\varepsilon > 0$*, if the instantaneous amplitude* $A(t)$ *and instantaneous phase* $\phi(t)$ *satisfy the following strongly modulated conditions*

$$|A''(t)| < \varepsilon, \quad |\phi'''(t)| < \varepsilon, \quad t \in R, \tag{21}$$

then the IF $\omega = \phi'(t)$ of the signal satisfies the following IF equation

$$\frac{\omega^2}{2\pi\alpha^2\phi''(t)}\Im\left\{\frac{\frac{\partial}{\partial t}S(t,\omega,c(t,\omega))}{S(t,\omega,c(t,\omega))}\right\} - \Re\left\{\frac{\frac{\partial}{\partial t}S(t,\omega,c(t,\omega))}{S(t,\omega,c(t,\omega))}\right\} = 0, \tag{22}$$

where $S(t,\omega,c(t,\omega))$ is the ASTCMW of the signal (6), $|S(t,\omega,c(t,\omega))| > r$, $r > 0$ is a constant and $\Re\{\cdot\}$ and $\Im\{\cdot\}$ are the real part and imaginary part of a complex number, respectively.

Proof According to (21), signal (6) around the point t can be expressed as

$$f(t+\tau) = (A(t) + A'(t)\tau)e^{j2\pi(\phi(t)+\phi'(t)\tau+\frac{\phi''(t)}{2}\tau^2)}. \tag{23}$$

Strictly, the expression above should be approximate equality, but for convenience purposes, exact equality is employed. Inserting (23) to (7), the ASTCMW can be represented as

$$S(t,\omega,c(t,\omega)) = \frac{|\omega|}{\sqrt{2\pi}\alpha}e^{j2\pi(\phi(t)-\omega t)}(A(t)\Gamma_0 + A'(t)\Gamma_1), \tag{24}$$

where $\Gamma_k = \int_{-\infty}^{+\infty}\frac{\tau^k}{k!}e^{-\frac{\omega^2\tau^2}{2\alpha^2}}e^{-j2\pi\frac{c(t,\omega)-\phi''(t)}{2}\tau^2}e^{-j2\pi(\omega-\phi'(t))\tau}\mathrm{d}\tau$, $k = 0, 1$.

Because $c(t,\omega) = \phi''(t)$ in the ASTCMW of a mono-component signal, Γ_k can be simplified to

$$\begin{aligned}\Gamma_k &= \int_{-\infty}^{+\infty}\frac{\tau^k}{k!}e^{-\frac{\omega^2\tau^2}{2\alpha^2}}e^{-j2\pi(\omega-\phi'(t))\tau}\mathrm{d}\tau \\ &= \frac{\alpha}{\omega}\int_{-\infty}^{+\infty}\frac{\tau^k\alpha^k}{k!\omega^k}e^{-\frac{\tau^2}{2}}e^{-j2\pi(\alpha-\frac{\phi'(t)\alpha}{\omega})\tau}\mathrm{d}\tau \\ &= \frac{j^k\alpha^{k+1}}{k!(2\pi)^k\omega^{k+1}}\widehat{\widetilde{g}}^{(k)}(\alpha - \frac{\phi'(t)\alpha}{\omega}),\end{aligned} \tag{25}$$

where $\widehat{\widetilde{g}}(\omega) = \sqrt{2\pi}e^{-2\pi^2\omega^2}$ is the Fourier transform of $\widetilde{g}(t) = e^{-\frac{t^2}{2}}$ and $\widehat{\widetilde{g}}^{(k)}(\omega)$ is the k-order derivative of $\widehat{\widetilde{g}}(\omega)$. Accordingly, (24) can be rewritten as

$$\begin{aligned}&S(t,\omega,c(t,\omega)) \\ &= e^{j2\pi(\phi(t)-\omega t)}e^{-2\pi^2\frac{\alpha^2}{\omega^2}(\omega-\phi'(t))^2}[A(t) - j2\pi A'(t)\frac{\alpha^2}{\omega^2}(\omega-\phi'(t))].\end{aligned} \tag{26}$$

It is followed that

$$\Re\left\{\frac{\frac{\partial}{\partial t}S(t,\omega,c(t,\omega))}{S(t,\omega,c(t,\omega))}\right\}=\frac{4\pi^2\phi''\alpha^2}{\omega^2}(\omega-\phi')+\frac{1}{\Delta}\left[AA'-4\pi^2(A')^2\frac{\alpha^4\phi''}{\omega^4}(\omega-\phi')\right],$$
$$\Im\left\{\frac{\frac{\partial}{\partial t}S(t,\omega,c(t,\omega))}{S(t,\omega,c(t,\omega))}\right\}=2\pi(\phi'-\omega)+\frac{2\pi}{\Delta}\left[AA'\frac{\phi''\alpha^2}{\omega^2}+(A')^2\frac{\alpha^2}{\omega^2}(\omega-\phi')\right], \tag{27}$$

where $\Delta = A^2+4\pi^2(A')^2(\frac{\alpha}{\omega})^4(\omega-\phi')^2$ and the argument t is omitted from $A(t)$, $A'(t)$, $\phi'(t)$ and $\phi''(t)$ for expression simplification.

According to (27), it is obvious that the IF $\omega=\phi'(t)$ satisfies equation (22).

$$\frac{\omega^2}{2\pi\alpha^2\phi''(t)}\Im\left\{\frac{\frac{\partial}{\partial t}S(t,\omega,c(t,\omega))}{S(t,\omega,c(t,\omega))}\right\}-\Re\left\{\frac{\frac{\partial}{\partial t}S(t,\omega,c(t,\omega))}{S(t,\omega,c(t,\omega))}\right\}=0.$$

The proof is completed. □

Utilizing IF equation (22), the synchroextracting transform based upon the ASTCMW (SET-ASTCMW) can be defined as

$$T(t,\omega)=S(t,\omega,c(t,\omega))\zeta(\omega-\hat{\omega}(t,\omega)), \tag{28}$$

where $S(t,\omega,c(t,\omega))$ and $\hat{\omega}(t,\omega)$ are the ASTCMW and the solution of equation (22) around the IF, respectively, and $\zeta(\omega-\hat{\omega}(t,\omega))$ is a synchroextracting operator defined as

$$\zeta(\omega-\hat{\omega}(t,\omega))=\begin{cases}1 & \omega=\hat{\omega}(t,\omega)\\ 0 & \text{otherwise}\end{cases}. \tag{29}$$

It is worth mentioning that if the IF of each component is separable, the proposed SET-ASTCMW is suitable for a multi-component signal.

To sum up, the detailed procedure of the SET-ASTCMW is displayed in Algorithm 2. The computational cost of the SET-ASTCMW mainly focuses on the ASTCMW and synchroextracting operator. For a signal with N samples, the ASTCMW requires $O(N_\theta N^2\log_2 N)$ operations. The computation of the synchroextracting operator is less than $O(N^2)$. Hence, the total computing complexity of the SET-ASTCMW is no more than $O(N_\theta N^2\log_2 N)$.

4 Experimental Validation

4.1 Performance of the Proposed Methods

In this subsection, the performance of the ASTCMW and SET-ASTCMW is examined using one real and three synthetic test signals. The energy concentration of the ASTCMW is compared with other advanced TFA methods, including the STFT, the ST [34], the CSK-ST [49], the Bi-Gaussian ST [26], and Moukadem's ST [20], which is a generalization of the modifications in [2,19,27,31,41] and has a better result than

Algorithm 2 SET-ASTCMW algorithm

Input signal $f(t)$, N_θ (i.e., the number of discrete θ), the frequency parameter α and positive constants r and ξ;
Calculate $\theta_n, n = 1, 2, \ldots, N_\theta$, from (12);
For each θ_n
Calculate the ASTCMW $S(t, \omega, \theta_n)$ from (13) and $\frac{\partial}{\partial t} S(t, \omega, \theta_n)$;
for each time–frequency point (t, ω)
  if $\max_{\theta_n} |S(t, \omega, \theta_n)| > r$
  Define $\widetilde{c}(t, \omega) = \arg\max_{\theta_n} |S(t, \omega, \theta_n)|$;
  Calculate $S(t, \omega, \widetilde{c}(t, \omega))$ and $\frac{\partial}{\partial t} S(t, \omega, \widetilde{c}(t, \omega))$;
    if $|\frac{\omega^2}{2\pi\alpha^2 \widetilde{c}(t,\omega)} \Im\{\frac{\frac{\partial}{\partial t} S(t,\omega,\widetilde{c}(t,\omega))}{S(t,\omega,\widetilde{c}(t,\omega))}\} - \Re\{\frac{\frac{\partial}{\partial t} S(t,\omega,\widetilde{c}(t,\omega))}{S(t,\omega,\widetilde{c}(t,\omega))}\}| < \xi$
     Define $Q(t, \omega) = 1$;
    end if
  end if
end for
for each time–frequency point (t, ω)
Calculate $T(t, \omega) = S(t, \omega, \widetilde{c}(t, \omega)) Q(t, \omega)$;
Output $T(t, \omega)$.

these modifications. Subsequently, the performance of the SET-ASTCMW is compared with the other five post-processing methods, i.e., the SST [10], the SSST [14], the SSGST [42], the Second-SST [22] and the SET [43].

4.1.1 Performance of the ASTCMW

A synthetic signal and a bat signal are used to demonstrate the performance of the ASTCMW. The synthetic signal consists of two LFM signals that have the same chirp rate, and the bat signal recorded by Rice University is widely used to test TFA methods.

The synthetic signal can be given as

$$\begin{aligned} f_{11}(t) &= e^{j80\pi t^2}, \\ f_{12}(t) &= e^{j80\pi t^2 + j18\pi t}, \\ f_1(t) &= f_{11}(t) + f_{12}(t), \qquad 0 \le t < 1. \end{aligned} \tag{30}$$

Its TFRs are shown in Fig. 4, and the ideal TFR is displayed in Fig. 4a. In Fig. 4, it is obvious that the result obtained by the ASTCMW taking proper parameters ($\alpha = 8$, $c(t, \omega) = 80$) has more concentrated energy representation and accurate TFR in the IF than other TFA methods, i.e., the ST (Fig. 4b), the STFT (Fig. 4c), Moukadem's ST (Fig. 4d), the CSK-ST (Fig. 4e) and the Bi-Gaussian ST (Fig. 4f). In Fig. 4g, the ASTCMW with $\alpha = 1$ and $c(t, \omega) = 80$, which can be considered as the ST with a complex-valued window [28], gives that the energy at low frequencies is more concentrated than at high frequencies. This is in accord with the analysis of α taken a low value in Sect. 2. Consequently, for LFM signals that have an invariable chirp rate, the ASTCMW has a more concentrated result in the time–frequency plane.

The bat signal is the echolocation signal emitted by a large brown bat, Eptesicus Fusus. By producing the frequency-modulated and sweeping-downward signal, and

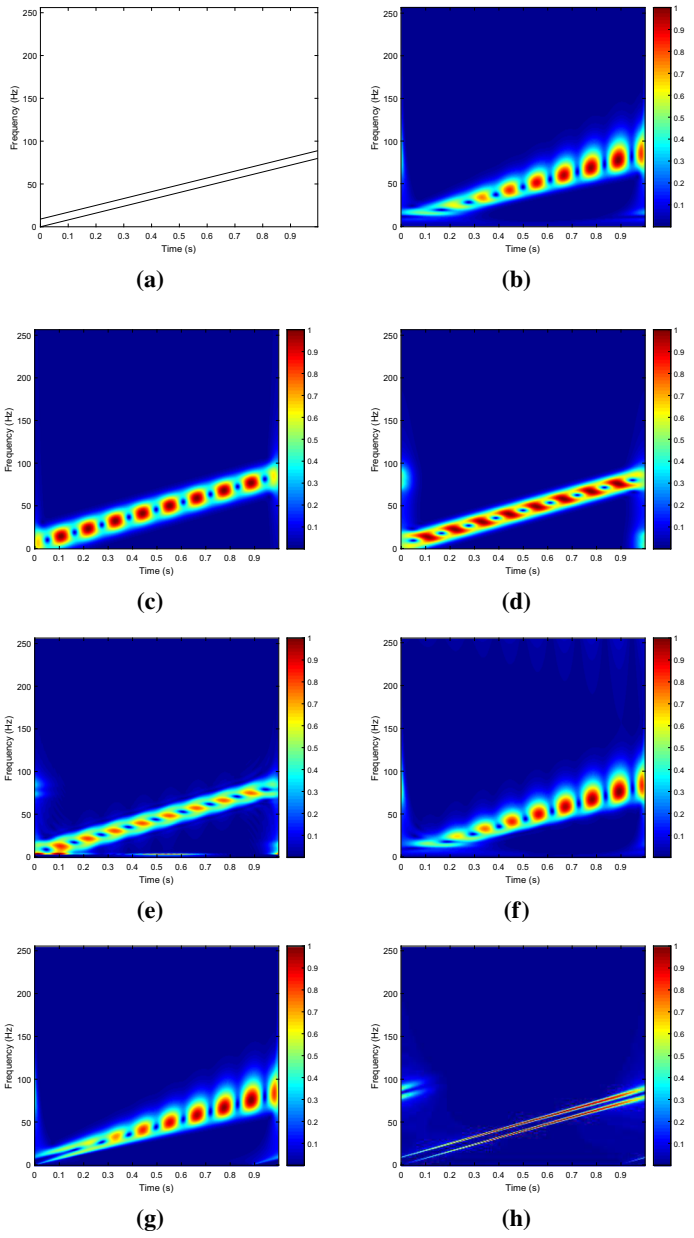

Fig. 4 TFRs of the signal (30). **a** The ideal TFR, **b** ST, **c** STFT, **d** Moukadem's ST, **e** CSK-ST, **f** Bi-Gaussian ST, **g** ASTCMW with $\alpha = 1$ and $c(t, \omega) = 80$, **h** ASTCMW with $\alpha = 8$ and $c(t, \omega) = 80$

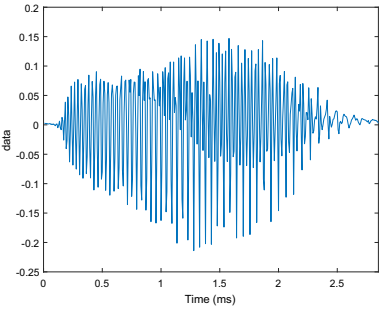

Fig. 5 The bat signal

collecting the echo-delay signal, the bats can identify the object in the environment. This signal is sampled at 400 points, and its sampling frequency is 140kHz [43]. The waveform of this signal and its TFRs are shown in Figs. 5 and 6, respectively. Figure 6a, d shows that the ST and the Bi-Gaussian ST provide poor energy concentration and worse resolution, especially at high frequencies. In Fig. 6c, the CSK-ST provides a poor frequency resolution than Moukadem's ST (Fig. 6e) and a poor time resolution than the ST. In Fig. 6e, Moukadem's ST provides the TFR similar to the STFT result (Fig. 6b). Compared with them, the ASTCMW gives a more concentrated TFR in the IF, as illustrated in Fig. 6f. This contrast of Moukadem's ST result and the ASTCMW result is explained in further detail, as shown in Fig. 6g, h. The ASTCMW result in Fig. 6h shows a narrower band around the IF track than Moukadem's ST result in Fig. 6g. A concentrated TFR in the IF will produce a better result in the further processing of signals. Accordingly, the proposed ASTCMW generates a satisfactory result.

4.1.2 Performance of the SET-ASTCMW

Two synthetic signals are used in the subsection to illustrate the performance of the SET-ASTCMW. They are a bi-component cross-signal and a strongly frequency-modulated signal whose first-order derivative of the amplitude with respect to t is equal to 0.

Firstly, the strongly frequency-modulated signal is given by

$$f(t) = \begin{cases} e^{-j10\pi \ln(-25t+1)} & -0.5 \le t \le 0 \\ e^{j10\pi \ln(25t+1)} & 0 < t < 0.5 \end{cases}. \tag{31}$$

For this signal, Fig. 7 presents the TFRs generated by six post-processing methods containing the SST based on the Gauss wavelet, the SSST, the Second-SST, the SSGST, the SET and the SET-ASTCMW. As shown in Fig. 7a, the SST result fails to give useful information at high frequencies. Compared with the SST, the SSST can generate a better result at high frequencies, as illustrated in Fig. 7b. However, the result obtained by the SSST is blurrier than the results generated by the Second-SST (Fig. 7c) and the SSGST (Fig. 7d). Compared with the Second-SST and the SSGST, the SET (Fig. 7e) and the SET-ASTCMW (Fig. 7f) give higher performance. Although the SET result

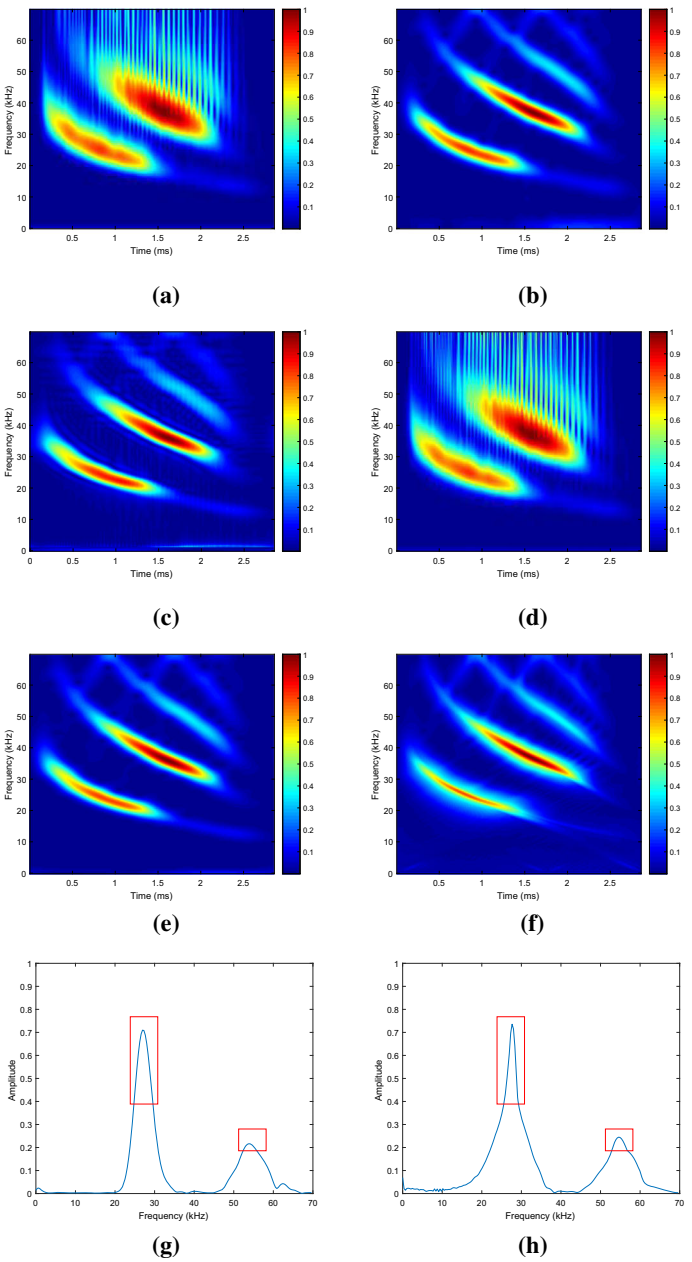

Fig. 6 TFRs of the bat signal. **a** ST, **b** STFT, **c** CSK-ST, **d** Bi-Gaussian ST, **e** Moukadem's ST, **f** ASTCMW with $\alpha = 4$ and $N_\theta = 12$. Time slices at 0.6ms from **g** Moukadem's ST result and **h** ASTCMW result

and the SET-ASTCMW result have a small difference, Fig. 7g, h shows that the TFR generated by the SET-ASTCMW has a more concentrated energy representation than the SET at 20Hz.

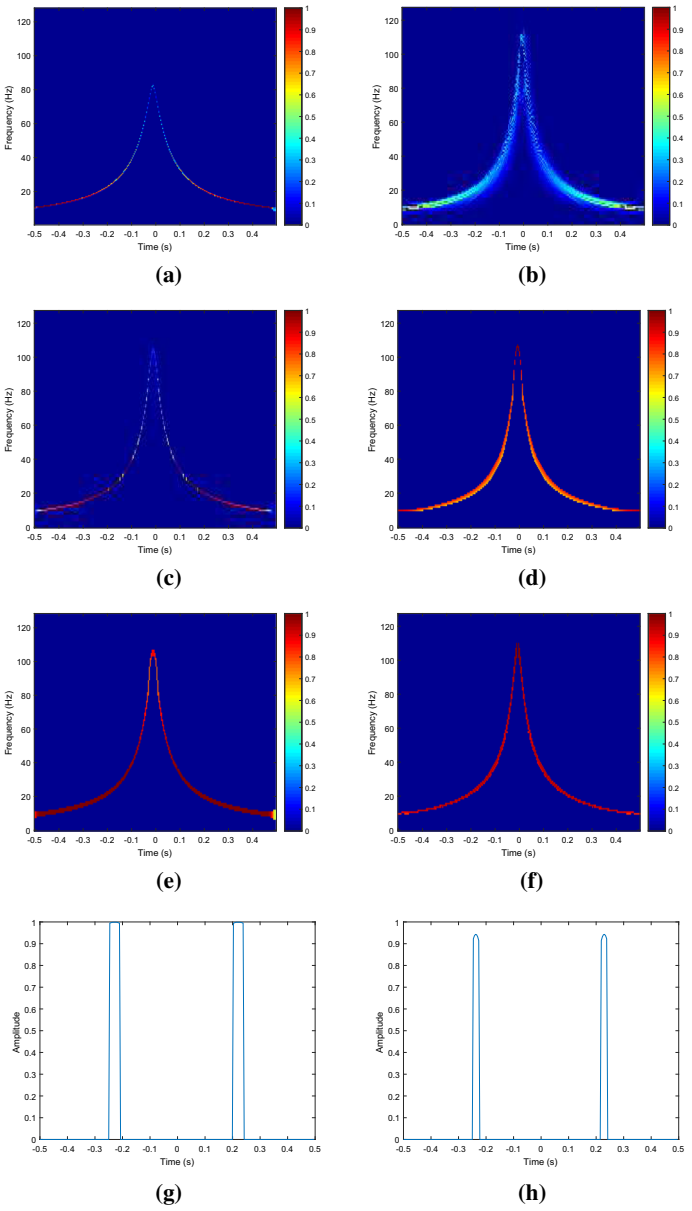

Fig. 7 TFRs of the strongly frequency-modulated signal. **a** SST, **b** SSST, **c** Second-SST, **d** SSGST, **e** SET, **f** SET-ASTCMW with $\alpha = 1$, $N_\theta = 20$ and $\xi = 0.18$. Frequency slices at 20Hz from **g** SET result and **h** SET-ASTCMW result

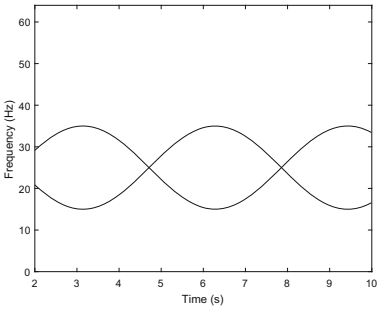

Fig. 8 Ideal TFR of the bi-component cross-signal

Secondly, another synthetic signal, the bi-component cross-signal, is expressed as

$$\begin{aligned} f_{21}(t) &= \sin(2\pi(25t - 10\sin t)), \\ f_{22}(t) &= \sin(2\pi(25t + 10\sin t)), \\ f_2(t) &= f_{21}(t) + f_{22}(t), \qquad 2 \le t \le 10. \end{aligned} \tag{32}$$

The ideal TFR of this signal is displayed in Fig. 8, and its TFRs generated by six post-processing methods, i.e., the SST, the SSST, the Second-SST, the SSGST, the SET and the SET-ASTCMW, are shown in Fig. 9. The SST and the SSST generate blurry results, as illustrated in Fig. 9a, b. Figure 9c, d shows that the Second-SST and the SSGST cannot provide effective information near the crossover point. Compared with the four methods mentioned above, the SET (Fig. 9e) and the SET-ASTCMW (Fig. 9f) have better results. The difference between the two, however, lies in the accuracy of the IF near the crossover point, as illustrated in Fig. 9g, h. More specifically, for the bi-component cross-signal, the SET-ASTCMW gives a more resolution result than the SET near the crossover point.

4.2 Effect of Additive White Noise

To test the robustness of the proposed methods, white noise is added in the signal (30), the bat signal, the strongly frequency-modulated signal and the bi-component cross-signal, and their TFRs are shown in Figs. 10, 11, 12, and 13, respectively. For the influence of the general random noise and modeling errors [11,35,37,46], it will be studied in future work.

White noise with SNR=2dB is added to the signal (30), and its TFRs are illustrated in Fig. 10. The ASTCMW (Fig. 10f) still provides a better concentration than other TFA methods, i.e., the ST (Fig. 10a), the STFT (Fig. 10b), the CSK-ST (Fig. 10c), the Bi-Gaussian ST (Fig. 10d) and Moukadem's ST (Fig. 10e). For the noisy bat signal with SNR=10dB, the ST (Fig. 11a) and the Bi-Gaussian ST (Fig. 11d) still suffer from poorer energy concentration than the other four methods. The ASTCMW (Fig. 11f) provides a more concentrated energy representation in the IF than the STFT (Fig. 11b) and the CSK-ST (Fig. 11c). The difference between Moukadem's ST (Fig. 11e) and the ASTCMW is the energy concentration in the IF, as displayed in Fig. 11g, h. The

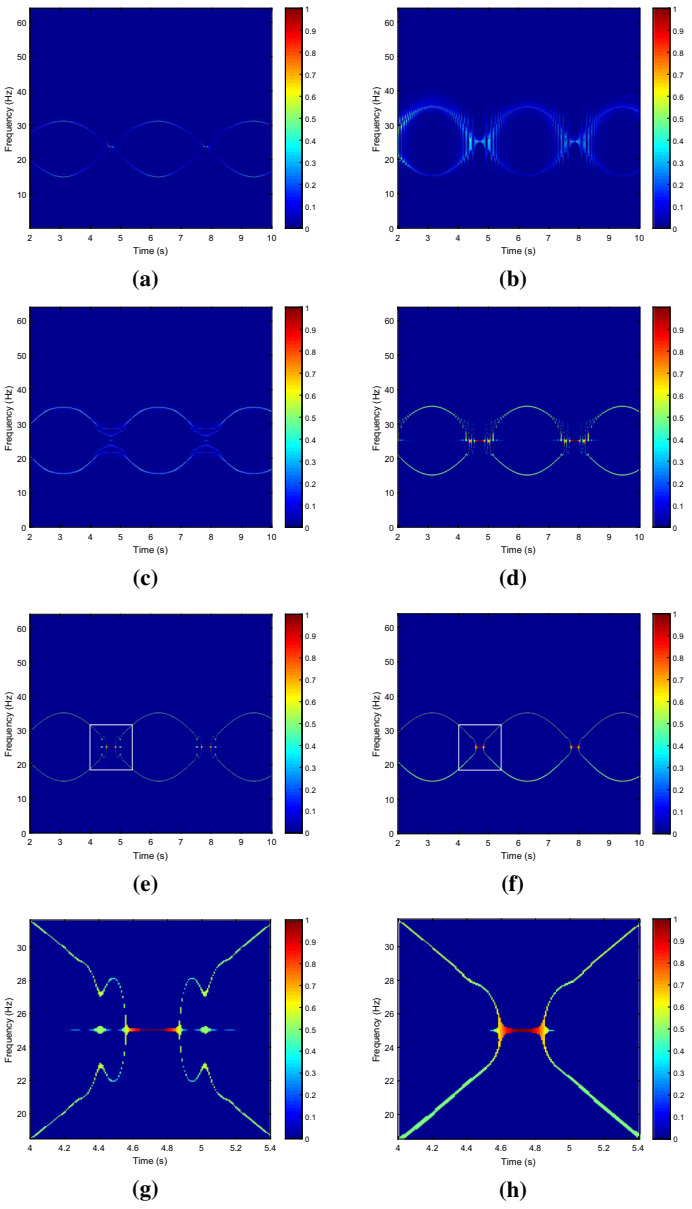

Fig. 9 TFRs of the bi-component cross-signal. **a** SST, **b** SSST, **c** Second-SST, **d** SSGST, **e** SET, **f** SET-ASTCMW with $\alpha = 2.32$, $N_\theta = 8$ and $\xi = 2$. **g** Result within the white rectangle of **e**. **h** Result within the white rectangle of **f**

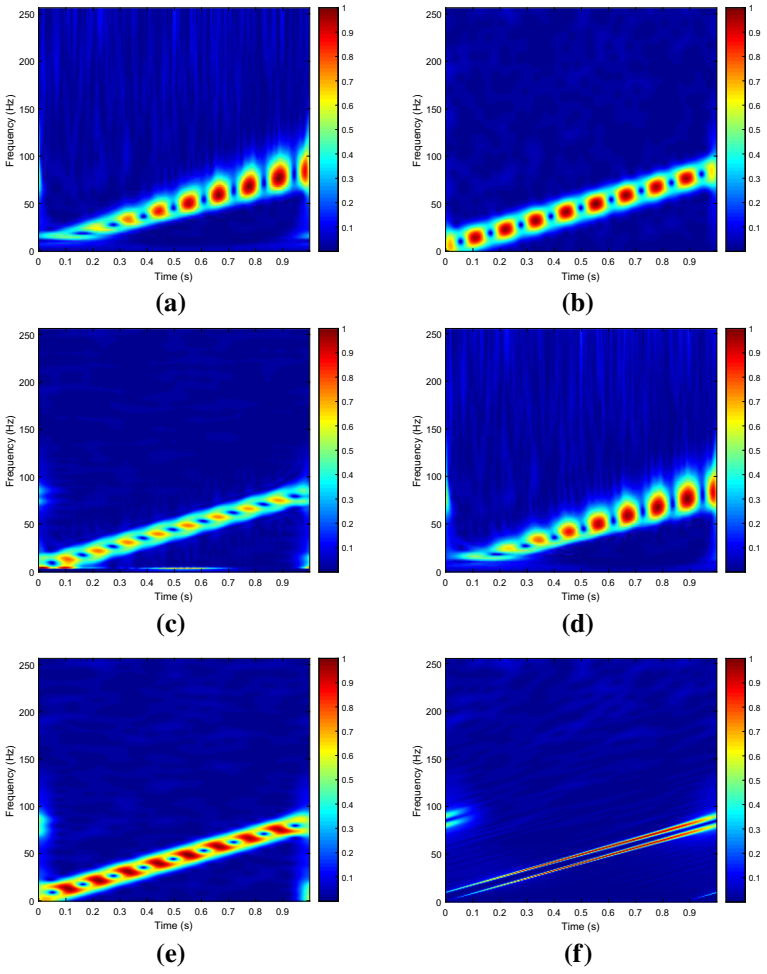

Fig. 10 TFRs of noisy signal (30) with SNR=2dB. **a** ST, **b** STFT, **c** CSK-ST, **d** Bi-Gaussian ST, **e** Moukadem's ST, **f** ASTCMW with $\alpha = 8$ and $c(t, \omega) = 80$

ASTCMW, therefore, gives a more concentrated energy representation in the IF among the six TFA methods.

The TFRs of the strongly frequency-modulated signal with SNR=1dB and the bi-component cross-signal with SNR=15dB are illustrated in Figs. 12 and 13, respectively. For the former, the SSST (Fig. 12b), the Second-SST (Fig. 12c), the SSGST (Fig. 12d), the SET (Fig. 12e) and the SET-ASTCMW (Fig. 12f) are more robust to noise than the SST (Fig. 12a). Moreover, the SET-ASTCMW gives a more resolution energy representation at low frequencies than the SET and higher energy in the IF than the Second-SST and the SSGST. Additionally, it provides a more concentrated energy representation all over the time–frequency plane than the SSST. For the noisy bi-component cross-signal with SNR=15dB, the noise cannot affect the advantage of the

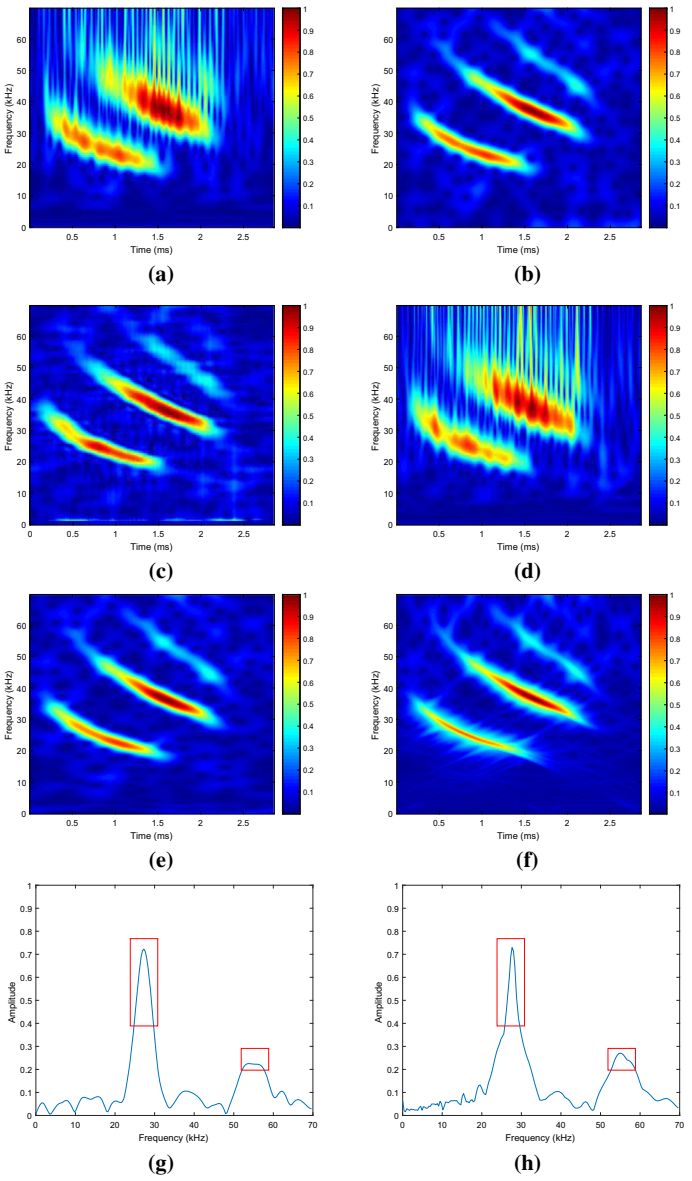

Fig. 11 TFRs of noisy bat signal with SNR=10dB. **a** ST, **b** STFT, **c** CSK-ST, **d** Bi-Gaussian ST, **e** Moukadem's ST, **f** ASTCMW with $\alpha = 4$ and $N_\theta = 12$. Time slices at 0.6ms from **g** Moukadem's ST result and **h** ASTCMW result

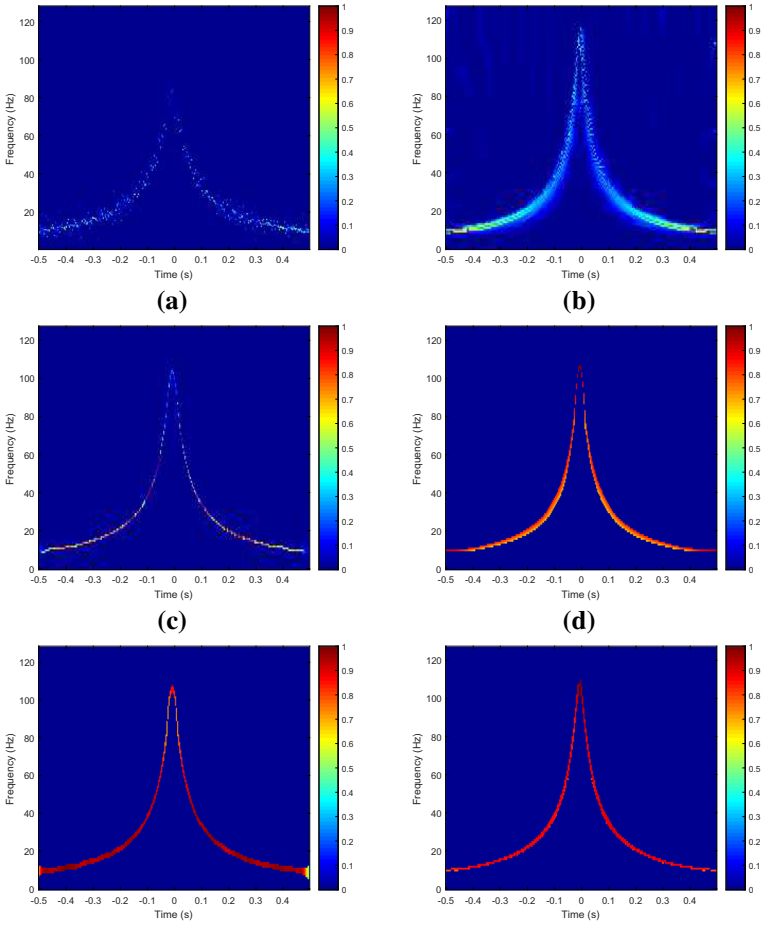

Fig. 12 TFRs of noisy strongly frequency-modulated signal with SNR=1dB. **a** SST, **b** SSST, **c** Second-SST, **d** SSGST, **e** SET, **f** SET-ASTCMW with $\alpha = 1$, $N_\theta = 20$ and $\xi = 0.18$

SET-ASTCMW near the crossover point comparing with the other five post-processing methods, as shown in Fig. 13. Furthermore, Fig. 14 shows the detected IF trajectories of noisy bi-component cross-signal from six post-processing methods, and that the noises have affected the detection of the IF. Although the Error1 (mean relative error [48] of mode $f_{21}(t)$) of detected IF by the SET-ASTCMW is greater than the SSGST and SET, the Error2 (mean relative error of mode $f_{22}(t)$) of detected IF by the SET-ASTCMW is the smallest among the six post-processing methods. On the whole, the comparative results again prove that the SET-ASTCMW has more satisfactory noise robustness than others.

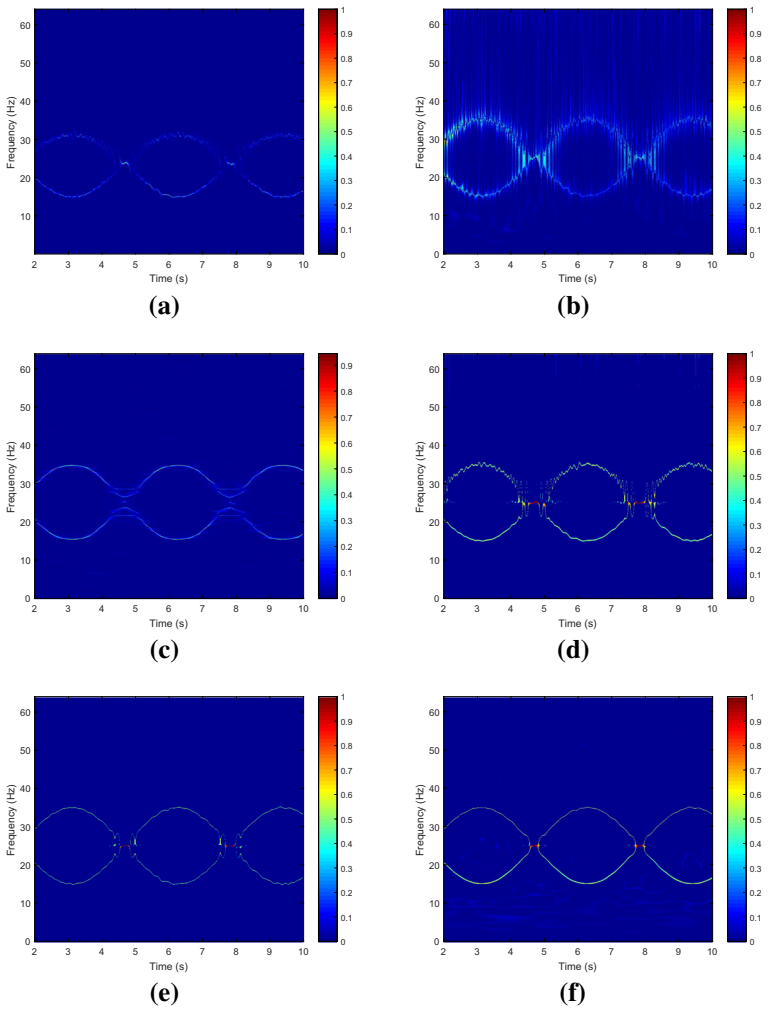

Fig. 13 TFRs of noisy bi-component cross-signal with SNR=15dB. **a** SST, **b** SSST, **c** Second-SST, **d** SSGST, **e** SET, **f** SET-ASTCMW with $\alpha = 2.32$, $N_\theta = 8$ and $\xi = 2$

5 Conclusion

In this paper, a new time–frequency analysis method, an adaptive S-transform with chirp-modulated window (ASTCMW), is proposed to enhance the energy concentration of the ST in the instantaneous frequency in the time–frequency plane. The chirp-modulated window contains two parameters, the chirp rate parameter and the frequency parameter. The former is estimated by optimizing the amplitude of the ASTCMW, and the optimizing method can be used to approximate the chirp rate of the input signal. The reference range of the latter is given by considering the chirp-modulated window as the fractional Fourier transform of a function. Nonetheless, in

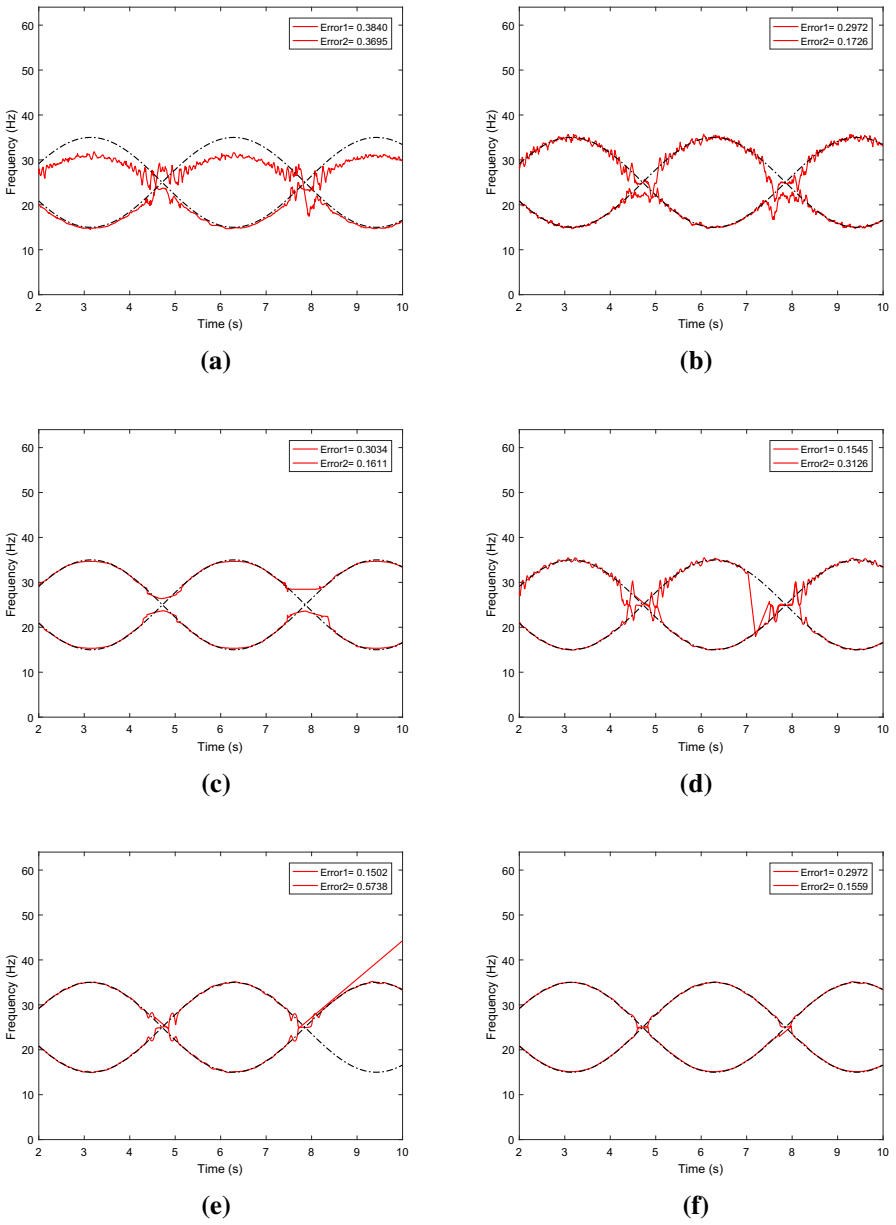

Fig. 14 IF estimation where the true IF is black—and the detected IF is red. Error1/Error2 denotes the mean relative error of mode $f_{21}(t)/f_{22}(t)$. **a** SST, **b** SSST, **c** Second-SST, **d** SSGST, **e** SET, **f** SET-ASTCMW

practical applications, the optimal frequency parameter should be selected based on the signal to be analyzed. Compared with common time–frequency analysis methods, the ASTCMW with appropriate frequency parameters has a better representation for linear frequency-modulated signals. To further improve the energy concentration of the ASTCMW of strongly modulated signals, the equation the instantaneous frequency satisfies based upon ASTCMW is found. On the basis of the equation, the synchroextracting transform based upon the ASTCMW (SET-ASTCMW) is developed. For the bi-component cross-signal, the SET-ASTCMW provides a more accurate instantaneous frequency feature near the crossover point by comparison with existing post-processing methods, and it is a more effective method dealing with a strongly modulated signal. Besides, there is a new idea embedded in this paper. That is using the rotation of the analysis window to improve the energy concentration in the time–frequency plane. The methods used in the paper may attract also other researchers in similar reduction approaches with applications in signal processing like second-order optimization methods for total variation, power system dynamic analysis [7–9]. In addition, it is worthwhile to provide a theoretical analysis of the ASTCMW and SET-ASTCMW in the future.

Acknowledgements This work was supported by National Natural Science Foundation of China under Grant U20B2075. The authors wish to thank the editor and the anonymous reviewers for their constructive comments and suggestions in improving the quality of the manuscript.

Data availability statement The datasets analyzed during the current study are available from the corresponding author on reasonable request.

Declarations

Conflict of interest The authors declare that they have no conflict of interest.

References

1. L.B. Almeida, The fractional Fourier transform and time-frequency representations. IEEE Trans. Signal Process. **42**(11), 3084–3091 (1994)
2. S. Assous, B. Boashash, Evaluation of the modified S-transform for time-frequency synchrony analysis and source localisation. EURASIP J. Adv. Signal Process. (2012). https://doi.org/10.1186/1687-6180-2012-49
3. B. Biswal, P.K. Dash, M. Biswal, Time frequency analysis and FPGA implementation of modified S-transform for de-noising. Int. J. Signal Process. Image Process. Pattern Recogn. **4**(2), 119–136 (2011)
4. R.A. Brown, M.L. Lauzon, R. Frayne, A general description of linear time-frequency transforms and formulation of a fast, invertible transform that samples the continuous S-transform spectrum nonredundantly. IEEE Trans. Signal Process. **58**(1), 281–290 (2010)
5. A. Bultheel, H. Sulbaran, Computation of the fractional Fourier transform. Appl. Comput. Harmon. Anal. **16**(3), 182–202 (2004)
6. L. Cohen, *Time-Frequency Analysis: Theory and Application* (Prentice Hall, Upper Saddle River, 1995)
7. I. Dassios, K. Fountoulakis, J. Gondzio, A preconditioner for a primal-dual Newton Conjugate Gradients method for Compressed Sensing problems. SIAM J. Sci. Comput. **37**(6), A2783–A2812 (2015)
8. I. Dassios, G. Tzounas, F. Milano, Generalized fractional controller for singular systems of differential equations. J. Comput. Appl. Math. (2020). https://doi.org/10.1016/j.cam.2020.112919

9. I. Dassios, G. Tzounas, F. Milano, Participation factors for singular systems of differential equations. Circuits Syst. Signal Process. **39**(1), 83–110 (2020)
10. I. Daubechies, J. Lu, H. Wu, Synchrosqueezed wavelet transforms: an empirical mode decomposition-like tool. Appl. Comput. Harmon. Anal. **30**(2), 243–261 (2011)
11. X. Dong, S. He, V. Stojanović, Robust fault detection filter design for a class of discrete-time conic-type non-linear Markov jump systems with jump fault signals. IET Contr. Theory Appl. **14**(14), 1912–1919 (2020)
12. P. Flandrin, F. Auger, E. Chassande-Mottin, *Time-Frequency Reassignment: From Principles to Algorithms, in Applications in Time-Frequency Signal Processing* (CRC, Arizona, 2003), pp. 179–203
13. A.V. Hirtum, D. Berckmans, Considering the influence of artificial environmental noise to study cough time-frequency features. J. Sound Vibr. **266**(3), 667–675 (2003)
14. Z. Huang, J. Zhang, T. Zhao, Y. Sun, Synchrosqueezing S-transform and its application in seismic spectral decomposition. IEEE Trans. Geosci. Remote Sens. **54**(2), 817–825 (2016)
15. K. Kodera, R. Gendrin, C. Villedary, Analysis of time-varying signals with small BT values. IEEE Trans. Acoust. Speech Signal Process. **26**(1), 64–76 (1978)
16. K. Kodera, C. Villedary, R. Gendrin, A new method for the numerical analysis of non-stationary signals. Phys. Earth Planet. Int. **12**(2–3), 142–150 (1976)
17. Z. Li, J. Gao, H. Li, Z. Zhang, N. Liu, X. Zhu, Synchroextracting transform: the theory analysis and comparisons with the synchrosqueezing transform. Signal Process. (2020). https://doi.org/10.1016/j.sigpro.2019.107243
18. Y. Liu, W. Zhou, P. Li, S. Yang, Y. Tian, An ultrahigh frequency partial discharge signal de-noising method based on a generalized S-transform and module time-frequency matrix. Sensors (2016). https://doi.org/10.3390/s16060941
19. L. Mansinha, R.G. Stockwell, R.P. Lowe, Pattern analysis with two-dimensional spectral localisation: applications of two-dimensional S transform. Phys. A **239**(1–3), 286–295 (1997)
20. A. Moukadem, Z. Bouguila, D.O. Abdeslam, A. Dieterlen, A new optimized Stockwell transform applied on synthetic and real non-stationary signals. Digit. Signal Process. **46**, 226–238 (2015)
21. A. Moukadem, A. Dieterlen, N. Hueber, C. Brandt, A robust heart sounds segmentation module based on S-transform. Biomed. Signal Process. Control **8**(3), 273–281 (2013)
22. T. Oberlin, S. Meignen, V. Perrier, Second-order synchrosqueezing transform or invertible reassignment? Towards ideal time-frequency representations. IEEE Trans. Signal Process. **63**(5), 1335–1344 (2015)
23. T. Oberlin, S. Meignen, V. Perrier, The Fourier-based synchrosqueezing transform, in *2014 IEEE International Conference on Acoustics, Speech and Signal Processing* (IEEE, 2014), pp. 315–319
24. Z.K. Peng, G. Meng, F.L. Chu, Z.Q. Lang, W.M. Zhang, Y. Yang, Polynomial chirplet transform with application to instantaneous frequency estimation. IEEE Trans. Instrum. Meas. **60**(9), 3222–3229 (2011)
25. C.R. Pinnegar, A new subclass of complex-valued S-transform windows. Signal Process. **86**(8), 2051–2055 (2006)
26. C.R. Pinnegar, L. Mansinha, The bi-Gaussian S-transform. SIAM J. Sci. Comput. **24**(5), 1678–1692 (2003)
27. C.R. Pinnegar, L. Mansinha, The S-transform with windows of arbitrary and varying shape. Geophysics **68**(1), 381–385 (2003)
28. C.R. Pinnegar, L. Mansinha, Time-local Fourier analysis with a scalable, phase-modulated analyzing function: the S-transform with a complex window. Signal Process. **84**(7), 1167–1176 (2004)
29. D. Pršić, N. Nedić, V. Stojanović, A nature inspired optimal control of pneumatic-driven parallel robot platform. Proc. Inst. Mech. Eng. Part C-J. Mech. Eng. Sci. **231**(1), 59–71 (2017)
30. M.J.B. Reddy, R.K. Raghupathy, K.P. Venkatesh, D.K. Mohanta, Power quality analysis using discrete orthogonal S-transform (DOST). Digit. Signal Process. **23**(2), 616–626 (2013)
31. E. Sejdić, I. Djurović, J. Jiang, A window width optimized S-transform. EURASIP J. Adv. Signal Process. (2008). https://doi.org/10.1155/2008/672941
32. H. Singh, R.K. Tripathy, R.B. Pachori, Detection of sleep apnea from heart beat interval and ECG derived respiration signals using sliding mode singular spectrum analysis. Digit. Signal Process. (2020). https://doi.org/10.1016/j.dsp.2020.102796
33. R.G. Stockwell, A basis for efficient representation of the S-transform. Digit. Signal Process. **17**(1), 371–393 (2007)

34. R.G. Stockwell, L. Mansinha, R.P. Lowe, Localization of the complex spectrum: the S transform. IEEE Trans. Signal Process. **44**(4), 998–1001 (1996)
35. V. Stojanović, S. He, B. Zhang, State and parameter joint estimation of linear stochastic systems in presence of faults and non-Gaussian noises. Int. J. Robust Nonlinear Control **30**(16), 6683–6700 (2020)
36. V. Stojanović, N. Nedić, D. Prsic, L. Dubonjic, V. Djordjevic, Application of cuckoo search algorithm to constrained control problem of a parallel robot platform. Int. J. Adv. Manuf. Technol. **87**(9–12), 2497–2507 (2016)
37. H. Tao, P. Wang, Y. Chen, V. Stojanović, H. Yang, An unsupervised fault diagnosis method for rolling bearing using STFT and generative neural networks. J. Frankl. Inst.-Eng. Appl. Math. **357**(11), 7286–7307 (2020)
38. X. Tu, Y. Hu, F. Li, S. Abbas, Z. Liu, W. Bao, Demodulated high-order synchrosqueezing transform with application to machine fault diagnosis. IEEE Trans. Ind. Electron. **66**(4), 3071–3081 (2019)
39. S. Ventosa, C. Simon, M. Schimmel, J.J. Dañobeitia, A. Mànuel, The S-transform from a wavelet point of view. IEEE Trans. Signal Process. **56**(7), 2771–2780 (2008)
40. B. Wang, Y. Yin, C. Yuan, P. Wang, An amplitude- and frequency-preserving S transform. IEEE Geosci. Remote Sens. Lett. (2020). https://doi.org/10.1109/LGRS.2020.2994135
41. L. Wang, X. Meng, An adaptive Generalized S-transform for instantaneous frequency estimation. Signal Process. **91**(8), 1876–1886 (2011)
42. Q. Wang, J. Gao, N. Liu, X. Jiang, High-resolution seismic time-frequency analysis using the synchrosqueezing generalized S-transform. IEEE Geosci. Remote Sens. Lett. **15**(3), 374–378 (2018)
43. G. Yu, M. Yu, C. Xu, Synchroextracting transform. IEEE Trans. Ind. Electron. **64**(10), 8042–8054 (2017)
44. G. Yu, Y. Zhou, General linear chirplet transform. Mech. Syst. Signal Process. **70–71**, 958–973 (2016)
45. K. Zhang, X. Chen, L. Liao, M. Tang, J. Wu, A new rotating machinery fault diagnosis method based on local oscillatory-characteristic decomposition. Digit. Signal Process. **78**, 98–107 (2018)
46. X. Zhang, S. He, V. Stojanović, X. Luan, F. Liu, Finite-time asynchronous dissipative filtering of conic-type nonlinear Markov jump systems. Sci. China-Inf. Sci. (2021). https://doi.org/10.1007/s11432-020-2913-x
47. D. Zhu, Q. Gao, D. Sun, Y. Lu, S. Peng, A detection method for bearing faults using null space pursuit and S transform. Signal Process. **96**, 80–89 (2014)
48. X. Zhu, Z. Zhang, J. Gao, B. Li, Z. Li, X. Huang, G. Wen, Synchroextracting chirplet transform for accurate IF estimate and perfect signal reconstruction. Digit. Signal Process. **93**, 172–186 (2019)
49. Z. Zidelmal, H. Hamil, A. Moukadem, A. Amirou, D. Ould-Abdeslam, S-transform based on compact support kernel. Digit. Signal Process. **62**, 137–149 (2017)